Structural analysis of circular UHPCC form for hybrid pier under construction loads

X.G. Wu[*1,2], X.Y. Zhao[2], and S.M. Han[3]

[1]*School of Civil Engineering, Harbin Institute of Technology, Harbin, China*
[2]*School of Architecture Engineering, Harbin Engineering University, Harbin, China*
[3]*School of Civil Engineering, Kumoh National Institute of Technology, Gumi, Korea*

Abstract. Ultra high performance cementitious composite material is applied to the design of multifunctional permanent form for bridge pier in this paper. The basic properties and calculating constitutive model of ultra high performance cementitious composite are introduced briefly. According to momental theory of thin-walled shell, the analytical solutions of structural behavior parameters including circumferential stress, longitudinal stress and shear stress are derived for UHPCC thin-walled circular tube. Based on relevant code of construction loads (MHURD of PPC 2008), the calculating parameter expression of construction loads for UHPCC thin-walled circular tube is presented. With geometrical dimensions of typical pier, the structural behavior parameters of UHPCC tube under construction loads are calculated. The effects of geometrical parameters of UHPCC tube on structural behavior are analyzed and the design advices for UHPCC tube are proposed. This paper shall provide a scientific reference for UHPCC permanent form design and UHPCC hybrid structure application.

Keywords: Ultra high performance cementitious composite; pier column; permanent form, construction loads

1. Introduction

Ultra high performance cementitious composite (UHPCC) is obtained by mixing short and thin steel fiber, high strength cementitious matrix, and mineral admixtures with special mixing technique and curing system. UHPCC exhibits high mechanical properties and durability properties with compressive strength 80~400 MPa, tensile strength 10~30 MPa, and elastic modulus 40~50 GPa. Therefore, the advanced material of UHPCC has many obvious superiors to improve structure performances and UHPCC will act as a new generation of engineering structural material by substituting normal strength concrete and normal high strength concrete in the future design (Wu and Xu 2009). Recently, researchers carried out extensive researching works and communications world widely including material strain hardening behavior (Wu and Han 2009), constitutive property behavior of UHPCC (Williams *et al* 2010), strength model(Ramadoss and Nagamani 2008), UHPCC behavior under multi-axial compression (Kittinun *et al* 2010), and interface performances of UHPCC hybrid elements (Wu and Han 2010), etc. Some new type structures using UHPCC were developed recently such as Shepherds bridge of Australian (Cavill *et al* 2003), Wapello bridge of Iowa in U.S.A. (Graybeal *et al* 2004), Kuyshu high speed bridge

---

* Corresponding author, Ph.D., E–mail: wuxiangguo@hit.edu.cn

made in Japan (Okuma 2004), FHWA short span bridge in U.S.A (Graybeal *et al* 2004), and Saint-Pierre-La-Cour hybrid bridge in France (Behloul 2007). The design of hybrid bridge deck with prefabricate UHPCC plate results in reduction of structures s.w. 2.2 times. The application of new type hybrid structure shows effectiveness on economies, construction speed, structural durability, and material-saving design.

The construction of gravity pier normally utilize steel cyclic formwork. However, installation and dismantlement of steel cyclic formwork consume amount of man hour. Traditional steel formwork cost is high due to the materials and out-back-haul problem. In addition, traditional gravity pier construction causes concrete surface to expose outside naturally after demold. Traditional gravity pier durability properties are lower especially for railway bridge pier. To improve the existed bridge pier service life, Railway Transportation Management Center of China proposed a design conception of pier protection plate which was already applied to existing railway bridge pier protection to improve existing structural durability (MREMC of P.P.C. 2009). A design conception of UHPCC hybrid structure is applied to the new type gravity pier in this paper. UHPCC permanent form holds some characteristics such as high strength, high durability and light weight. UHPCC permanent form acts as formwork at bridge pier construction stage, as protection plate at the post construction stage, and also as coat layer of interior reinforced steel. Hence this new form is named as multifunctional permanent formwork.

UHPCC circular form behavior under construction loads is one of the main issues in the new hybrid pier design. Based on plate and shell theory, the structural behaviors of UHPCC circular form under construction loads are studied theoretically including circumferential cracking, longitudinal extrusion responses, and root segment flexure behavior. These studies may lay a reference or design basis for UHPCC circular permanent form for circular pier and new type of UHPCC hybrid pier application. Corresponding structural tests and the study of UHPCC hybrid pier structure behaviors are presented in the following-up paper.

2. Concepts of UHPCC

Compared with normal cement concrete (NCC) and fiber reinforced concrete (FRC), UHPCC holds ultra high strength, ductile behavior under tension and bending, and high durability (MREMC of P.P.C. 2009). Table 1 shows the comparisons of UHPCC properties with those of NCC and FRC.

The resistance ability of chloride attack of UHPCC is about two Coulombs based on ASTM 1202 which is rather higher than NCC and FRC. The resistance of freezing-thawing is also very high with almost 100 percent of relative dynamic elastic modulus remaining after 600 cycles according to ASTM C 666B. Table 2 shows the comparisons of UHPCC durability items with NCC and HSC.

UHPCC consists of cement, silica fume, sand, fiber, water and superplasticizer. Typical water/cement-

Table 1 Mechanical properties comparison of UHPCC with NCC and FRC

Property	NCC	FRC	HSC	HSFRC	UHPCC
Compressive strength(MPa)	21-30	30-50	40-60	60-80	80-400
Flexural strength(MPa)	1-3	5-15	5-10	10-15	15-60
E-modulus(MPa)	21,000-35,000	30,000-40,000	30,000-40,000	40,000	< 50,000
Behavior characteristics	Brittle	Quasi Brittle	Brittle	Ductile	Ductile
Crack characteristics	Partial	Partial + Multiple	Partial	Partial + Multiple	Multiple

Table 2 Durability comparison of UHPCC with NCC and HSC

Property		NCC	HSC	UHPCC	Measurement
Resistance of Chloride attack (Coulombs)		2,445	178	2	ASTM C 1202
Neutralization (depth: mm, 6 month)		17	3.5	0	CO_2 10%, RH 60%, 30°C
Resistance of Freezing-Thawing (Relative Dynamic Elastic Modulus: %, 600 cycles)		78	95	100	ASTM C 666 B
Permeability	Air permeability (X10-16m^2)	0.1335	0.0475	0.01	Direct Pressure
	Water Permeability (mm^2/sec·Bar)	0.00362	0.00259	0.000472	
	Permeability (Coulombs)	776	135	1.1	ASTM C 1202
Porosity (ml/g)		0.1605	0.0874	0.0515	Auto Pore 9220

Table 3 Physical and chemical properties of cement and mineral admixture

Item Type	Surface area (cm^2/g)	Density (g/cm^3)	Ig.loss (%)	Chemical composition (%)		
				MgO	SO$_3$	SiO$_2$
Cement	3,333	3.14	1.40	2.8	2.3	-
Silica Fume	200,000	2.10	1.50	0.1	-	96.0

ratios are 0.15 to 0.20 with 20% to 30% of silica fume.

Ordinary portland cement and silica fume for admixture were used in the experiment. Their physical and chemical properties are shown in Table 3.

Domestic river sand with grain size of 0.5mm and below, density 2.62 g/cm^3, SiO$_2$ 93% was used as fine aggregate, and coarse aggregate was not used. Polycarboxylic ether-type super plasticizers with density of 1.01 g/cm^3 and 30% of solid ingredient in dark brown liquid were used. Domestic production of filling powders(silica flour) with average grain size of 100 μm was used which chemical properties are shown in Table 4.

High elastic steel fiber with parameters density 7.5 g/cm^3, length 13 mm, diameter 0.2 mm, and ultimate tensile strength 2,500 MPa were used here to increase the toughness with concrete volume fraction ratio 2%.

Mix compositions of UHPCC is shown in Table 5. Steel fiber mixing volume fraction is 2% of the composites. Mixing technique of UHPCC is shown in Figure 1.

Uniaxial compression and direct tension test results are shown in Figures 2(a) and 2(b). The average compression strength is 130 MPa with ultimate compressive strain 0.0038. There has obvious strain

Table 4 Chemical properties of filling powders

Size (μm)	Ig.loss (%)	Chemical composition (%)				
		Al$_2$O$_3$	MgO	CaO	Fe$_2$O$_3$	SiO$_2$
100	0.01	0.15	0.003	0.004	0.01	99.3
10	0.01	0.15	0.004	0.03	0.01	99.3

Table 5 Mix compositions of UHPCC (kg/m^3)

Cement	Silica fume	Filling powder	Fine sand	Super Plast.	Water	Expan. agent	Defoamer	Steel fiber
789.75	197.44	157.95	868.72	31.59	197.44	3.95	3.95	102.41

Fig. 1 Mixing process of UHPCC

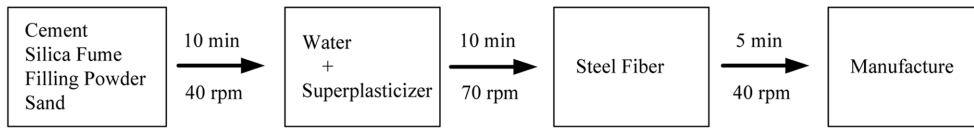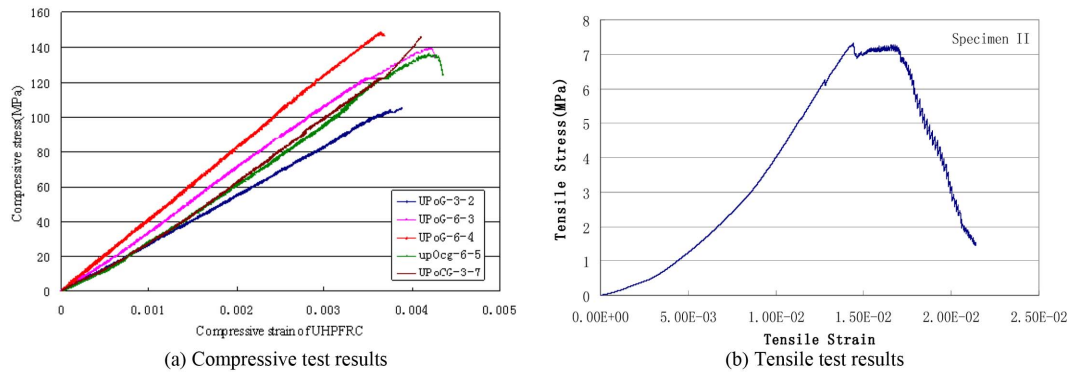| (a) Compressive test results | (b) Tensile test results |

Fig. 2 Test results of UHPCC

hardening behavior at the post cracking stage. The first cracking strength is 6~7 MPa and the ultimate tensile strength is about 7~8 MPa. There is an obvious strain "yielding" region and multiple cracking behavior.

3. Theoretical model of UHPCC circular thin-walled permanent form

Basic assumptions: (1) UHPCC is isotropic and homogeneous. (2) The boundary condition between UHPCC circular tube and foundation is fixed connection. (3) The design limit state is defined as macro-crack occurrence on the outside surface of UHPCC tube.

3.1 Stress-strain relation of UHPCC under axial compression and tension

The initial stage of stress and strain relation of UHPCC under axial compression shows quasi linear elastic behavior. Yielding elongation occurs after macro-crack occurrence with the axial compressive strength f_{ucy} and axial compressive strain ε_{ucy}. Due to fiber reinforcement, fiber debonding and pull-out phenomena continue at the yielding platform. UHPCC stress can be increased and local hardening behavior may occur which is resulted by geometrical dimension of axial compression member. The simplified computional model of UHPCC under axial compression is shown in Fig. 3. Linear secant modulus E_{uc0} of UHPCC can be measured with the initial cracking load and initial cracking strain.

As shown in the direct tension test results from figure, the stress-strain of UHPCC under uniaxial tension can be divided into four parts as shown in Fig. 4(a).

The first part is quasi linear elastic stage before the initial cracking stress. Initial micro-crack of material exists in UHPCC matrix in this stage. As increasing load, these initial cracks will propagate
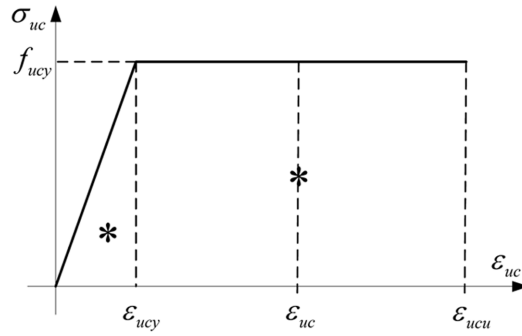
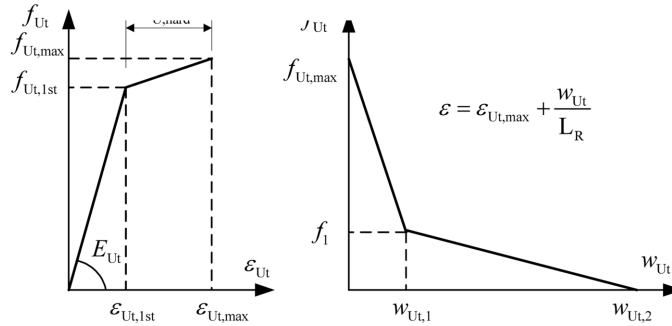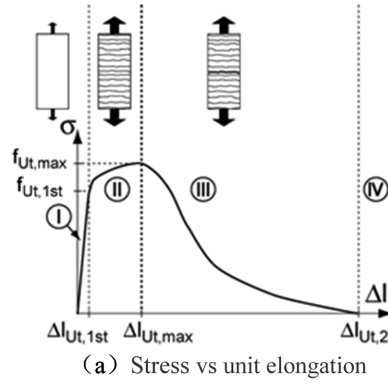Fig. 3 Simplified uniaxial compression constitutive relation of UHPCC

（a）Stress vs unit elongation

（b）Simplified uniaxial tension constitution of UHPCC

Fig. 4 Stress-strain of UHPCC under uniaxial tension

and connect each other. With bridging of steel fiber, the rigidness of the material is almost invariable.The second part is strain hardening stage. In this stage, micro-crack is developed as macro-crack and the material rigidness will be decreased obviously. Under the fiber reinforcement, material is deformed as multiple cracking behaviors. The third one is soften stage. In this stage, deformation will be localized as one single crack or several local cracks which is related with energy dissipation capability of each macro-crack. Fiber pulling-out and debonding behaviors are accompanied in the process of localized deformation. Finally, structural element will failure as one single main crack.The

Table 6 Parameters of UHPCC tensile constitutive model

Parameter	$f_{Ut,1st}$	$\varepsilon_{Ut,1st}$	$f_{Ut,max}$	$\varepsilon_{Ut,max}$	E_{Ut}	f_1	$w_{Ut,1}$	$w_{Ut,2}$	L_R
Value	6~8 MPa	0.0001	15 MPa	0.002~0.004	50 GPa	2.5 MPa	2 mm	6.5 mm	270 mm

last part is fiber pulling-out stage in which fiber pulling-out will be ended in localized crack. Material is in fracture state without any stress and structural element is failed in fracture.

Uniaxial tensile constitution of UHPCC is shown in Fig. 4(b) and the expression is shown in Eq. (1). The model parameters of corresponding axial tension test are shown in Table 6.

$$f = \begin{cases} E_{Ut}\varepsilon & 0 < \varepsilon \le \varepsilon_{Ut,1st} \\ \left(f_{Ut,max} - f_{Ut,1st}\right)\varepsilon / \varepsilon_{U,hard} & \varepsilon_{Ut,1st} < \varepsilon \le \varepsilon_{Ut,max} \\ \left(f_1 - f_{Ut,max}\right)\varepsilon / \left(w_{Ut,1}/L_R\right) & \varepsilon_{Ut,max} < \varepsilon \le \varepsilon_{Ut,max} + w_{Ut,1}/L_R \\ -f_1 L_R \varepsilon / \left(w_{Ut,2} - w_{Ut,1}\right) & \varepsilon_{Ut,max} + w_{Ut,1}/L_R < \varepsilon \le \varepsilon_{Ut,max} + w_{Ut,2}/L_R \end{cases} \tag{1}$$

3.2 Solutions of thin-walled circular tube of UHPCC

3.2.1 Theoretical model

The circular tube is assumed as model with upper non-restraint end and lower fixed boundary. Internal filling is new pouring concrete as shown in Fig. 5(a). One element P is selected for mechanics analysis of UHPCC circular tuber under loading model $q_n(x)$ and the corresponding stress state is shown in Fig. 5(b).

Here, t is the wall thickness of UHPCC tube, H is the height of the tube element, and R is radius of
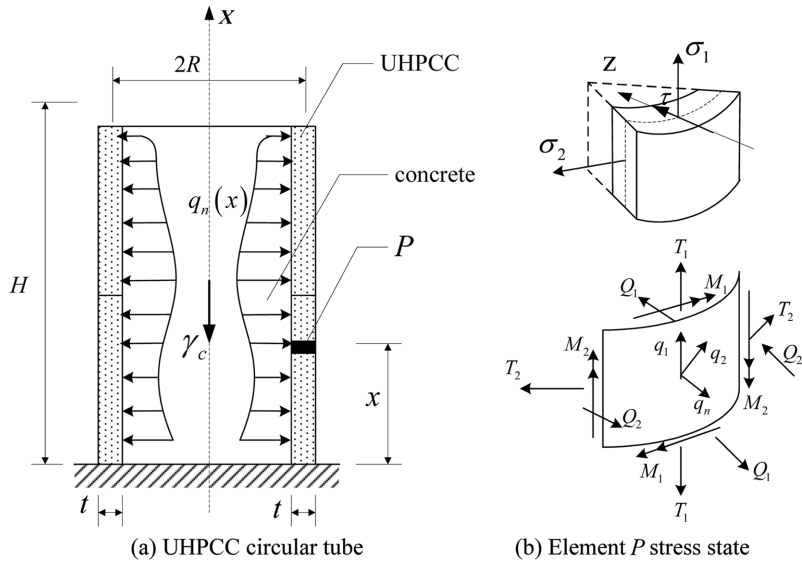

(a) UHPCC circular tube   (b) Element P stress state

Fig. 5 Stress state of UHPCC circular tube model

middle surface. γ_c is the gravity density of concrete. $q_n(x)$ is the load model acting as the internal surface of UHPCC tube.

According to momental elasticity theory of thin-walled circular tube(Timoshenko *et al* 1959), the internal force component of element P can be expressed as

$$\begin{cases} T_1 = \gamma_u t(H-x), T_2 = Et\dfrac{w}{R} + \mu T_1 \\[2mm] M_1 = D\dfrac{d^2 w}{dx^2}, M_2 = \mu M_1 \\[2mm] Q_1 = D\dfrac{d^3 w}{dx^3} \end{cases} \tag{2}$$

In which, γ_u is the gravity density of UHPCC. x is the longitudinal coordinate of P. μ is the Poisson ratio of UHPCC, and E is the elastic modulus of UHPCC which is equal to E_{Ut} measured from the uniaxial tensile test. β and D are two parameters for computation and the corresponding expressions can be written as

$$\beta = \frac{\sqrt[4]{3\left(1-\mu^2\right)}}{\sqrt{Rt}} \tag{3}$$

$$D = \frac{Et^3}{12\left(1-\mu^2\right)} \tag{4}$$

$q_m(x)$ is a combinatorial term for computation and can be expressed as

$$q_m\left(x\right) = q_n\left(x\right) - \frac{\mu}{R}T_1 \tag{5}$$

From the momental elasticity theory thin-walled circular tube, the normal displacement w of element P can be derived as

$$w = \frac{R^2}{Et}\left\{q_m\left(x\right) + e^{-\beta x}\left[-q_m\left(0\right)\cos\beta x + \left(-\frac{q_m{}'\left(0\right)}{\beta} - q_m\left(0\right)\right)\sin\beta x\right]\right\} \tag{6}$$

$$= \frac{R^2}{Et}\left[q_m\left(x\right) + A_1 f_1\left(x\right) + A_2 f_2\left(x\right)\right]$$

Here, $f_1\left(x\right) = e^{-\beta x}\cos\beta x$, $f_2\left(x\right) = e^{-\beta x}\sin\beta x$, $A_1 = -q_m\left(0\right)$, and $A_2 = -\dfrac{q_m{}'\left(0\right)}{\beta} - q_m\left(0\right)$.

By substituting Eq. (6) into Eq. (2), the components of Eq. (2) can be obtained as

$$
\begin{cases}
T_2 = R\left[q_m(x) + A_1 f_1(x) + A_2 f_2(x)\right] + \mu T_1 \\[2mm]
M_1 = \dfrac{DR^2}{Et}\left[q_m''(x) + 2\beta^2 A_1 f_2(x) - 2\beta^2 A_2 f_1(x)\right] \\[2mm]
Q_1 = \dfrac{DR^2}{Et}\left[q_m'''(x) + 2\beta^2 B_1 f_2(x) - 2\beta^2 B_2 f_1(x)\right]
\end{cases} \tag{7}
$$

In which, $B_1 = -q_m'(0)$ and $B_2 = q_m'(0) + 2\beta q_m(0)$.

3.2.2 Basic solution

Circumference stress σ_2 and longitudinal stress σ_1 at any element P are assumed as linear distribution along the Z direction of tube thickness, i.e. the linear function of z. According to elasticity theory, these stress components can be expressed as

$$
\begin{cases}
\sigma_1 = \dfrac{T_1}{t} - \dfrac{M_1 z}{t^3/12} \\[2mm]
\sigma_2 = \dfrac{T_2}{t} - \dfrac{M_2 z}{t^3/12} \\[2mm]
\tau = \dfrac{Q_1}{t}
\end{cases} \tag{8}
$$

It can be seen that the circumference stress and longitudinal stress reach corresponding extremes at the internal and outside surfaces and the maximum stress components can be expressed as

$$
\begin{cases}
\sigma_1 = \dfrac{T_1}{t} \pm \dfrac{M_1}{t^2/6} \\[2mm]
\sigma_2 = \dfrac{T_2}{t} \pm \dfrac{M_2}{t^2/6}
\end{cases} \tag{9}
$$

By substituting (7) into (9), the maximum stress component can be written as

$$
\sigma_1 = \gamma_U (H - x) + \dfrac{6DR^2}{Et^3}\left[q_m''(x) + 2\beta^2 A_1 f_2(x) - 2\beta^2 A_2 f_1(x)\right] \tag{10}
$$

$$
\sigma_2 = \dfrac{R}{t}\left[q_m(x) + A_1 f_1(x) + A_2 f_2(x)\right] + \mu\dfrac{T_1}{t}
$$
$$
+ \dfrac{6DR^2}{Et^3}\left[q_m''(x) + 2\beta^2 A_1 f_2(x) - 2\beta^2 A_2 f_1(x)\right] \tag{11}
$$

$$
\tau = \dfrac{DR^2}{Et^2}\left[q_m'''(x) + 2\beta^2 B_1 f_2(x) - 2\beta^2 B_2 f_1(x)\right] \tag{12}
$$

3.3 Limit state of UHPCC permanent tube form

For linear load, $q_m''(x) \equiv 0$, and Eq. (11) can be simplified as

$$
\begin{aligned}
\sigma_2 = \frac{R}{t}\Big[q_m(x) + A_1 f_1(x) + A_2 f_2(x)\Big] + \frac{\mu T_1}{t} \\
+ \frac{12 D \beta^2 R^2}{E t^3}\Big[A_1 f_2(x) - A_2 f_1(x)\Big]
\end{aligned}
\tag{13}
$$

Let $\sigma_2 = f_{Ut,1st}$, the safety margin of circumference initial cracking state of UHPCC tube can be written as

$$
\begin{aligned}
M(x|R,t,H) = f_{Ut,1st} - \frac{R}{t}\Big[q_m(x) + A_1 f_1(x) + A_2 f_2(x)\Big] + \frac{\mu T_1}{t} \\
+ \frac{12 D \beta^2 R^2}{E t^3}\Big[A_1 f_2(x) - A_2 f_1(x)\Big]
\end{aligned}
\tag{14}
$$

In which, $f_{Ut,1st}$ is the initial cracking strength of UHPCC (MPa). The limit state equation of circumference initial cracking for UHPCC tube can be expressed as

$$
M(x|R,t,H) = 0
\tag{15}
$$

4. Construction load model for UHPCC permanent form

According to the regulation about construction load of JGJ162-2008(MHURD of PPC 2008), q_n can be expressed as $q_n = 1.2G_k + 1.4Q_k$ in which G_k and Q_k are lateral static compression load and pouring live load, respectively. When internal vibrator is used, the lateral compression load standard value G_k from new pouring concrete can be calculated from Eq. (16).

$$
F = \min\Big(0.22 g_c t_0 b_1 b_2 V^{\frac{1}{2}}, g_c(H_0 - x)\Big)
\tag{16}
$$

Here, F is the lateral compression value of new pouring concrete on the form (kN/m^2), γ_c is the gravity density of concrete (kN/m^3), V is the pouring speed of concrete (m/h). t_0 is initial setting time of new pouring concrete (h) which can be determined by experiment or by the recommended formula $t_0 = 2001(T + 15)$ for lacking of experiment statistics. T is the Celsius temperature of concrete. β_1 is a modified coefficient of admixture which is equal to 1.0 when there has no any admixture and is equal to 1.2 when retarder is added. β_2 is an modified coefficient for concrete slump constant effect and is equal to 0.85 when the slump constant is less than 30 mm and is equal to 1.00 when the slump constant is about 50-90 mm, and is equal to 1.15 when the slump constant is about 110~150 mm. H_0 is the total height of new pouring concrete (m).

The pouring live load Q_k is dependent on the feeding method in the form, which is equal to 2 kN/m^2 when down spouting, tumbling barrel, or tremor method is utilized, is equal to 4 kN/m^2 when carrier with capacity of 0.2~0.8 m^3 is utilized, and is equal to 6 kN/m^2 when carrier with capacity greater than 0.8 m^3 is utilized. The computational distribution diagram of concrete lateral compressive force is drawn
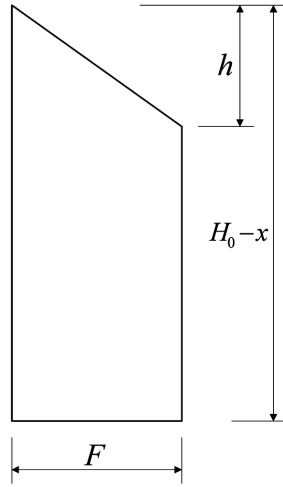
Fig. 6 Model of Construction Loads

as shown in Fig. 6 in which $h = F/\gamma_c$ and is the effective fall head of concrete.
Now, the computational combined item of construction load can be expressed as

$$q_m(x) = \min\left(0.264\gamma_c t_0 \beta_1 \beta_2 V^{\frac{1}{2}}, 1.2\gamma_c(H_0 - x)\right) + 1.4Q_k - \frac{\mu\gamma_u t}{R}(H - x) \qquad (17)$$

Let $x = 0$, the boundary value of the computational combined item of load can be written as

$$q_m(0) = \min\left(0.264\gamma_c t_0 \beta_1 \beta_2 V^{\frac{1}{2}}, 1.2\gamma_c H_0\right) + 1.4Q_k - \frac{\mu\gamma_U t}{R}H \qquad (18)$$

5. Results and analysis

Typical hybrid piers with dimensions $H = 10$ m, $R = 1.5$ m, and UHPCC wall thickness t = 2.5 cm, 3 cm, 4 cm, 5 cm are analyzed to determine the structural behaviors and corresponding parameters of UHPCC tube under construction loads. Load coefficients and material parameters are $\beta_1 = 1.2$, $\beta_2 = 1.0$, $t_0 = 5.7$ h, $V = 6$ m/h, $Q_k = 2$ kN/m^2, $\mu = 0.2$, $E_{uc} = 50$ GPa, $\gamma_c = 25$ kN/m,^{3} $\gamma_{uc} = 30$ kN/m^3, $H_0 = 2$ m and $f_{U/t,1st} = 6$ MPa. All the coefficients and parameters were described as above. For conservative safety design, the new pouring concrete height is assumed to be equal to the structural total height, i.e. the height of hardened concrete part is considered into the computational height of fresh pouring concrete. The calculation results are tabulated in Table 7 including longitudinal stress, circumferential stress, shear stress and normal displacement on inside surface and outside surface. Here, "*IS*" and "*OS*" are the abbreviations of inside and outside boundaries.

The parameters influence on stress and displacement of UHPCC tube under constructional load are analyzed with the Figure 7~11.

5.1. Distribution of longitudinal stress

Longitudinal stress σ_l is the coupling action of T_l and M_l. From the calculation results of Fig. 7(a)

Table 7 Calculation results of the typical UHPCC tube based on the proposed theoretical model

	x(mm) \ t(mm)	0	263	526	789	1053	1316	1579	1842	2105	4737	6842	10000
σ_1(IS) (MPa)	25	12.2350	−2.1001	0.0996	0.3581	0.2683	0.2582	0.2528	0.2448	0.2368	0.1579	0.0947	0.0000
	30	10.2330	−1.7652	−0.0709	0.3639	0.2809	0.2569	0.2522	0.2449	0.2369	0.1579	0.0947	0.0000
	40	7.7300	−1.1969	−0.2932	0.3184	0.3071	0.2612	0.2503	0.2445	0.2370	0.1579	0.0947	0.0000
	50	6.2291	−0.7802	−0.3931	0.2425	0.3178	0.2721	0.2507	0.2434	0.2368	0.1579	0.0947	0.0000
σ_1(OS) (MPa)	25	−11.6350	2.6843	0.4688	0.1945	0.2686	0.2629	0.2525	0.2447	0.2369	0.1579	0.0947	0.0000
	30	−9.6327	2.3494	0.6393	0.1887	0.2560	0.2642	0.2531	0.2446	0.2368	0.1579	0.0947	0.0000
	40	−7.1300	1.7811	0.8616	0.2342	0.2297	0.2598	0.2549	0.2450	0.2367	0.1579	0.0947	0.0000
	50	−5.6291	1.3644	0.9615	0.3101	0.2191	0.2489	0.2546	0.2460	0.2369	0.1579	0.0947	0.0000
σ_2(IS) (MPa)	25	2.4471	5.4250	7.0221	6.8279	6.7947	6.8026	6.8030	6.8028	6.8028	6.8028	5.8522	0.1680
	30	2.0465	4.1928	5.8385	5.7242	5.6613	5.6669	5.6693	5.6691	5.6690	5.6690	4.8768	0.1400
	40	1.5460	2.7560	4.2907	4.3461	4.2573	4.2465	4.2510	4.2520	4.2518	4.2517	3.6576	0.1050
	50	1.2458	1.9764	3.3221	3.5037	3.4262	3.3975	3.3987	3.4012	3.4016	3.4014	2.9261	0.0840
σ_2(OS) (MPa)	25	−2.3271	6.3819	7.0959	6.7952	6.7948	6.8035	6.8030	6.8028	6.8028	6.8028	5.8522	0.1680
	30	−1.9265	5.0157	5.9806	5.6892	5.6563	5.6684	5.6695	5.6690	5.6690	5.6690	4.8768	0.1400
	40	−1.4260	3.3516	4.5216	4.3292	4.2418	4.2462	4.2519	4.2521	4.2518	4.2517	3.6576	0.1050
	50	−1.1258	2.4053	3.5930	3.5172	3.4065	3.3928	3.3994	3.4017	3.4016	3.4014	2.9261	0.0840
τ (MPa)	25	−0.6687	0.0225	0.0179	−0.0019	−0.0004	0.0001	0.0000	0.0000	0.0000	0.0000	0.0000	0.0000
	30	−0.6094	0.0054	0.0240	−0.0006	−0.0009	0.0000	0.0000	0.0000	0.0000	0.0000	0.0000	0.0000
	40	−0.5262	−0.0223	0.0302	0.0039	−0.0015	−0.0004	0.0001	0.0000	0.0000	0.0000	0.0000	0.0000
	50	−0.4692	−0.0423	0.0308	0.0090	−0.0009	−0.0009	−0.0001	0.0001	0.0000	0.0000	0.0000	0.0000
w (mm)	25	0.0000	0.1754	0.2101	0.2027	0.2022	0.2025	0.2026	0.2026	0.2027	0.2031	0.1750	0.0050
	30	0.0000	0.1364	0.1756	0.1695	0.1682	0.1685	0.1686	0.1686	0.1687	0.1691	0.1457	0.0042
	40	0.0000	0.0899	0.1305	0.1285	0.1259	0.1258	0.1260	0.1261	0.1261	0.1266	0.1092	0.0032
	50	0.0000	0.0640	0.1020	0.1037	0.1009	0.1003	0.1005	0.1006	0.1006	0.1011	0.0872	0.0025

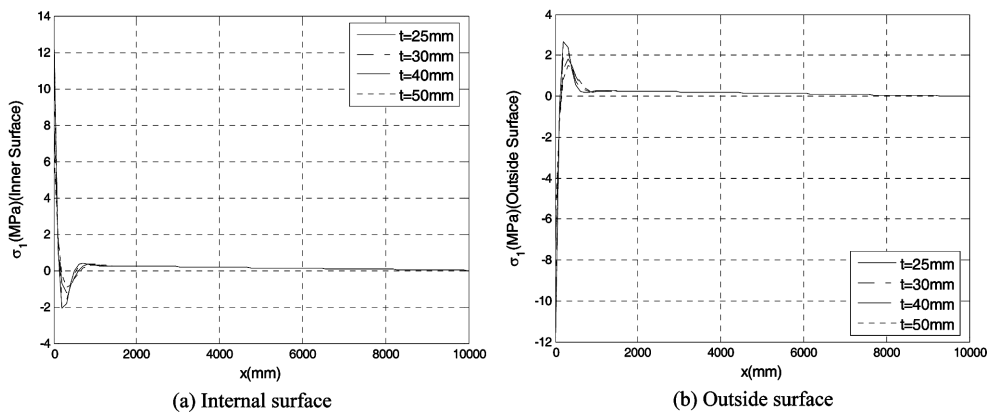
(a) Internal surface   (b) Outside surface

Fig. 7 Distribution of longitudinal stress

and (b), the longitudinal stress is in compression on the internal surface of the tube at the distance of 0.2 m ~0.4 m from the tube end. Corresponding stress on the outside surface is in tension. The compressive
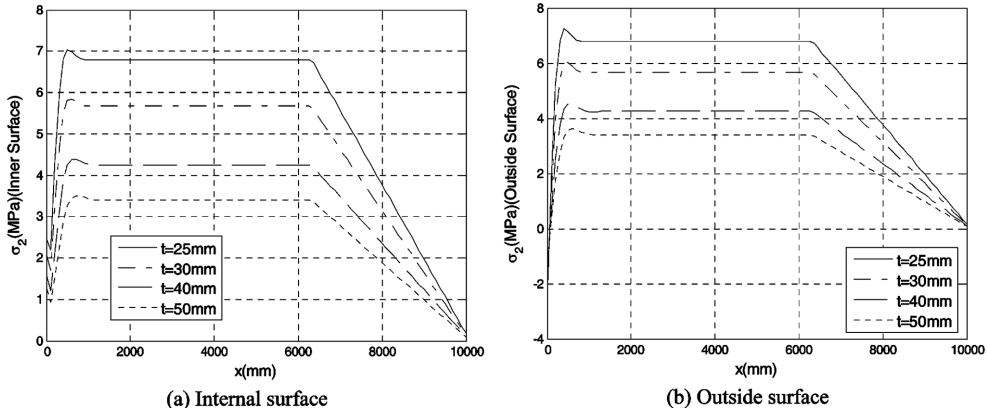
(a) Internal surface   (b) Outside surface

Fig. 8 Distribution of circular stress

stress and tensile stress are extreme. As the coordinate close to the end boundary, σ_1 is increasing which is tensile stress on the internal surface and compressive stress on the outside surface. Along the longitudinal coordinate direction of x, the longitudinal stress σ_1 approaches zero rapidly. As increasing of t, the absolute value of the stress decrease whether on the internal surface or on the outside surface.

5.2 Distribution of the circumferential stress

The circumferential stress σ_2 is the coupling action of T_2 and M_2. From the calculation results of the Fig. 8, the circumferential stress on internal and outside surfaces decrease gradually with the increasing of t. Whether on the internal surface or on the outside surface, the extreme value of the circumferential stress occurs at the distance 0.4~0.6 m from the tube end where the circumferential stress decreases slowly. In the region of the distance 3.5m-4m from the upper end, the stress decreases rapidly. For the thin-walled circular tube of UHPCC with $t = 2.5$ cm, the extreme circumferential stress is about 7.0~7.2 Mpa which is greater than the initial cracking strength 6.0-7.0MPa. For the thin-walled circular tube of UHPCC with $t = 3.0$ cm, the extreme circumferential stress is about 5.8~6.0 MPa and this thickness is the minimal design thickness based on total fall head assumption.

5.3 Distribution of the shear stress

Shear stress τ is resulted by N_1. From the calculation results of Fig. 9, the shear stress is a small quantity.

5.4 Normal displacement

Normal displacement w, a main deformation parameter of UHPCC tube, is shown in Fig. 10. From the results, middle part is control deformation region along the direction of the longitudinal axial x. The deformation approaches zero gradually at a certain region close to the upper and low end. The maximal deformation occurs in the region of 0.4~0.6 m from the low end. The maximal circumferential stress exists in this region. The distribution of the normal displacement along x is in accordance with the distribution of the circumferential stress long x. With the increasing of t, the normal displacement descends.
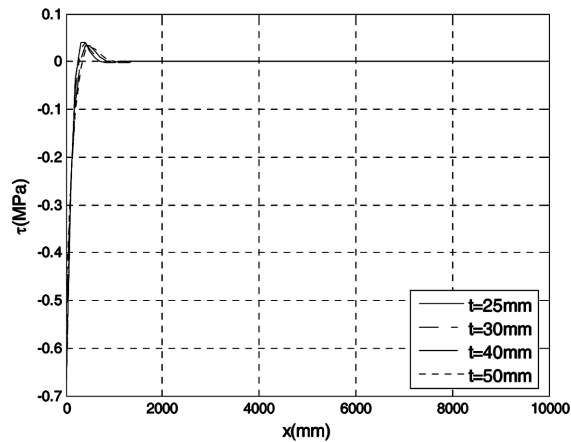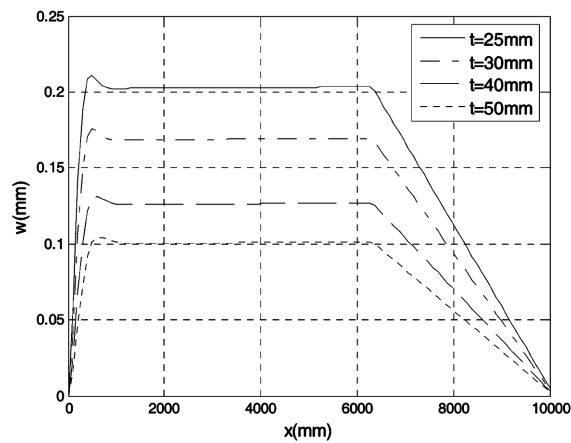
Fig. 9 Distribution of shear stress

Fig. 10 Distribution of normal displacement

For the case of $t = 5$ cm, the maximal deformation is about 0.105 mm which is only 0.22 percent of the wall thickness. For the case of $t = 2.5$ cm, the maximal deformation is about 0.21 mm which is 0.84 percent of the wall thickness.

6. Conclusions

Circumferential stress is a control design stress component for construction safety design of UHPCC tube. The stress is extreme at the distance 0.4 m~0.6 m from the lower end. For structural safety consideration, distributed slipping stirrup should be installed in the region of 0.4 m~0.6 m and the state of the stress extreme distribution in this region can be improved. According to the stress distributions, the minimum design thickness is advised as 3.0 cm for hybrid pier column structure of UHPCC tube.

The distribution of normal displacement is in accordance with the circumferential stress. According to the structural deformation consideration, the minimum design thickness is also advised as 3.0 cm for

hybrid pier column structure of UHPCC.

Compared with the mechanical properties of UHPCC, the longitudinal stress is a small quantity on the internal and outside surface. Hence the influence of this stress component can be omitted for design. The shear stress component is also a small quantity, can be omitted.

Acknowledgements

References

Behloul, M. (2007), "HPFRCC field of applications: Ductal recent experience", 5th High Performance Fiber Reinforced Cement Composite (HPFRCC5), Mainz, Germany, July.

Cavill, B. and Chirgwin, G. (2003), "The worlds first Ductal road bridge Sherpherds gully creek bridge, NSW", 21st Biennial Conference of the Concrete Institute of Australia, Brisbane.

Graybeal, B., Hartamann, J., and Perry, V. (2004), "Ultra-high performance concrete for highway bridge", FIB Symposium, Avignon, 26-28 April.

Kittinun S., Sherif E.T., and Gustavo P.M. (2010), "Behavior of high performance fiber reinforced cement composite under multi-axial compressive loading", *Cement Concrete Comp.*, **32**, 62-72.

MHURD of PPC(The Ministry of Housing and Urban-Rural Development of P.P.C.)(2008), *Technical Code for Safety of Forms in Construction(JGJ 162-2008)*, China Architecture & Building Press, Beijing.(In Chinese)

MREMC of PPC(Engineering Management Center of The Ministry of Railways of P.P.C.) (2009), *Constructurn Manual For Reactive Powder Concrete Member*, China Railway Publishing House, Beijing. (In Chinese)

Okuma, H., et al.(2006), "The first highway bridge applying ultra high strength fiber reinforced concrete in Japan", 7th International Conference on short and medium span bridge. Montreal, Canada.

Ramadoss P. and Nagamani, K. (2008), "A new strength model for the high-performance fiber reinforced concrete", *Comp. Concrete*, **5**(1), 21-36.

Timoshenko, S. P. and Woinowsky, K.S. (1959), *Theory of Plates and Shells*, McGraw-Hill Book Com., INC.

Williams, E.M., Graham, S.S., Akers, S.A., Reed P.A. and Rushing T.S. (2010), "Constitutive property behavior of an ultra-high-performance concrete with and without steel fibers", *Comp. Concrete*, **7**(2), 191-202.

Wu, X.G. and Han, S.M. (2009), "Multiple cracking model of fiber reinforced high performance cementitious composite under uniaxial tension", *Int. J. Concrete Struct. Mater.*, **3**(1), 71-77.

Wu, X.G. and Han, S.M. (2010), "Interface shear connection analysis of Ultrahigh-Performance fiber-Reinforced concrete composite girders", *J. Bridge Eng. (ASCE),* **15**(5), 493-502.

Wu, X.G. and Xu, S.L (2009), "Ultra high performance Cementitious hybrid and flexural analysis of the UHPCC-NC hybrid structure with full shear connection", *Key Engineering Materials*, 405-406, 69-74.

CC

Notation

f_{ucy}	the axial compressive strength of UHPCC
ε_{ucy}	the axial compressive strain
E_{uc0}	the linear secant modulus of UHPCC
$f_{Ut,1st}$	the first cracking strength of UHPCC
$f_{Ut,max}$	the ultimate tensile strength of UHPCC
$\varepsilon_{Ut,1st}$	the first cracking strain of UHPCC
$\varepsilon_{Ut,max}$	the ultimate tensile strain of UHPCC
E_{Ut}	the initial linear elasticity modulus of UHPCC
f_1	the inflexion strength in tensile soften region of UHPCC
$w_{Ut,1}$	the tensile displacement corresponding to the inflexion strength
$w_{Ut,2}$	the ultimate tensile displacement
L_R	the measurement length of dog bone specimen for UHPCC tension test
$q_n(x)$	internal loading distribution model
t	the wall thickness of UHPCC tube
H	the height of the tube element
R	the middle surface radisu of UHPCC tube
γ_c	the gravity density of concrete
γ_u	the gravity density of UHPCC
x	the longitudinal coordinate
μ	Poisson ratio of UHPCC
β and D	two computational parameters
w	the normal displacement
σ_2	circumference stress
σ_1	longitudinal stress
G_k	the lateral static compression load
Q_k	the pouring live load
F	the lateral compression value of new pouring concrete on the form
V	the pouring speed of concrete
t_0	the initial setting time of new pouring concrete
T	the Celsius temperature of concrete
β_1	modified coefficient of admixture
β_2	modified coefficient for concrete slump constant effect
H_0	the total height of new pouring concrete